Advance in Orientation Microscopy: Quantitative Analysis of Nanocrystalline Structures

Martin Seyring,[†] Xiaoyan Song,[‡] and Markus Rettenmayr[†,*]

[†]Institute of Materials Science and Technology, Friedrich Schiller University, D-07747 Jena, Germany and,[‡]College of Materials Science and Engineering, Beijing University of Technology, Beijing 100124, People's Republic of China

ABSTRACT The special properties of nanocrystalline materials are generally accepted to be a consequence of the high density of planar defects (grain and twin boundaries) and their characteristics. However, until now, nanograin structures have not been characterized with similar detail and statistical relevance as coarse-grained materials, due to the lack of an appropriate method. In the present paper, a novel method based on quantitative nanobeam diffraction in transmission electron microscopy (TEM) is presented to determine the misorientation of adjacent nanograins and subgrains. Spatial resolution of <5 nm can be achieved. This method is applicable to characterize orientation relationships in wire, film, and bulk materials with nanocrystalline structures. As a model material, nanocrystalline Cu is used. Several important features of the nanograin structure are discovered utilizing quantitative analysis: the fraction of twin boundaries is substantially higher than that observed in bright-field images in the TEM; small angle grain boundaries are prominent; there is an obvious dependence of the grain boundary characteristics on grain size distribution and mean grain size.

KEYWORDS: transmission electron microscopy (TEM) · orientation microscopy · nanobeam diffraction (NBD) · grain boundary analysis · nanograin structure · nanocrystalline Cu

Nanocrystalline metals exhibit favorable properties such as ultrahigh yield and fracture strengths as well as superior wear resistance, compared to their coarse-grained counterparts.[1,2] However, when the structure−property relationships are discussed, the discussion frequently remains qualitative. As an example, nanocrystalline copper (nc-Cu) is known to substantially change its properties with decreasing mean grain size. nc-Cu with a high density of nanotwins features increased mechanical strength together with preserved ductility,[3] electrical conductivity,[4] and thermal stability.[5] These special properties are attributed to the high density of boundaries and their characteristics,[6−9] but only selected aspects of the underlying mechanisms are specified. Additionally, the thermal stability of nanocrystalline structures is dependent on the properties of the grain boundaries that affect grain boundary migration.[10,11] If not impurity-controlled, the grain boundary mobility is a distinct function of the misorientation of adjacent grains.[10] Furthermore, the structural, electrical, and optical properties of nanowires[12,13] and nanocrystalline films[14,15] depend on the features of the nanoscale grain boundaries. A thorough characterization of nanoscale grain boundaries including some statistics is not available in the literature, mainly due to a lack of a powerful characterization method on the relevant length scale. Detailed analysis of the relationship between grain boundary structure and a nanomaterial's mechanical behavior or its thermal stability is clearly needed to achieve a more quantitative understanding of properties that are intrinsic to the nanoscaled structure and to control and optimize its performance.[16]

In this article, we introduce a precise method to analyze misorientation relationships of adjacent nanograins, allowing a grain boundary characterization in ultra-fine-grained nanocrystalline materials with grain sizes as low as ~10 nm. Electron backscatter diffraction (EBSD) in the scanning electron microscope (SEM), the most common grain orientation evaluation method, does at present not offer the opportunity to analyze ultra-fine-grained nanocrystalline materials. Under ideal conditions, the spatial resolution of EBSD is material-dependent, between 30 and 50 nm,[17,18] and resolution on the order of 20 nm was also reported.[19] However, EBSD cannot be extended to even smaller length scales, as Kikuchi diffraction (inelastic scattering) does not occur in the small volume of a nanocrystal.[20]

Convergent beam diffraction techniques in transmission electron microscopy (TEM) reach far below this length scale. Nanobeam diffraction (NBD) with a beam diameter down to 1 nm offers the possibility of crystallographic analysis of single nanograins

* Address correspondence to m.rettenmayr@uni-jena.de.

Received for review September 7, 2010 and accepted March 4, 2011.

Published online March 04, 2011
10.1021/nn1023126

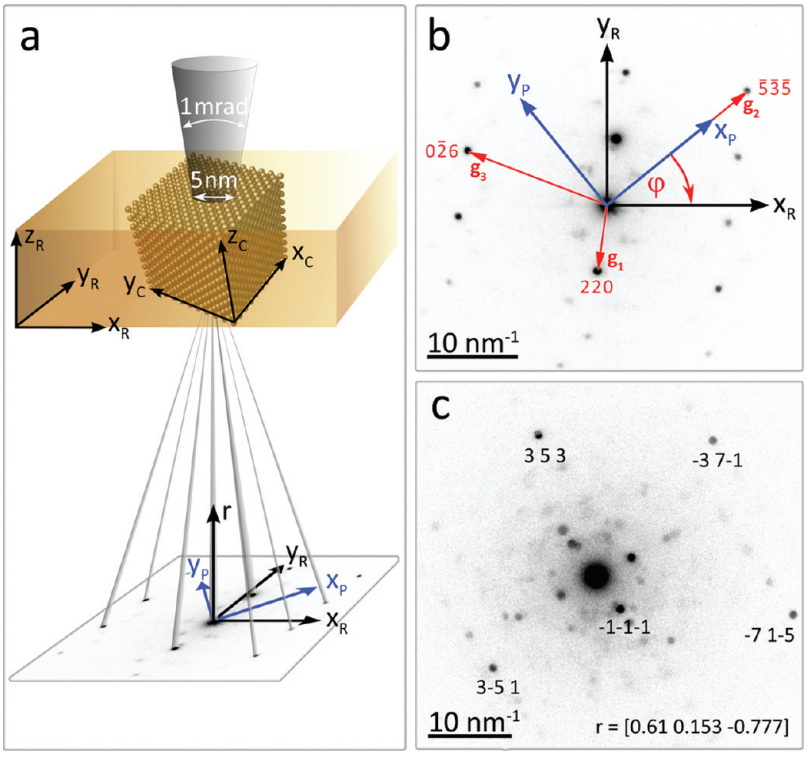

Figure 1. Principle of the NBD analysis: (a) schematic representation of the NBD analysis method for determining the orientation matrix of a grain from its NBD pattern; (b) three selected and indexed diffraction vectors $g_1 \ldots g_3$ are used to calculate the normal direction r, defining the pattern frame (x_P, y_P, r) that is rotated around φ along r to the reference frame (x_R, y_R, r); (c) example of indexed NBD pattern from an arbitrarily oriented nanocrystal.

with a spatial resolution of 1 nm.[21−23] However, determining even a single misorientation relationship of two adjacent grains from diffraction patterns with the conventional procedure is quite cumbersome because only regular zone axis patterns are straightforward to analyze; thus, the two grains to be analyzed need to be oriented (simultaneously or sequentially) in a crystallographic zone axis with respect to the electron beam by tilting the sample. This is accompanied by particular difficulties: it is not possible to observe its NBD pattern while tilting the sample, and it is a demanding task to track a nanograin during tilting because the nanograins move on the viewing screen and change their contrast and contours. The conventional procedure is so time-consuming that large numbers of grains will not be analyzed.

Three approaches that, in principle, are suitable for analyzing orientations in nanocrystalline structures in the TEM are documented in the literature. Orientation maps can be obtained (i) by dark-field conical scanning and orientation determination of reconstructed diffraction patterns from dark-field images,[24−28] (ii) by scanning a sample with a convergent beam while recording convergent beam electron diffraction (CBED) patterns,[29] (iii) by applying the D-STEM[20,30−32] technique with a nearly parallel nanobeam allowing a spatial resolution of 3 nm. Compared to D-STEM, the CBED technique offers the higher azimuthal accuracy,[29,33] but the larger convergence angle 2α limits the spatial resolution. Until now, all of these techniques were applied to analyze local texture in nanoscale materials. To the best of the authors' knowledge, these techniques have so far not been applied to analyze grain boundaries in nanocrystalline materials.

The method presented here applies NBD for orientation determination of single nanograins. It performs consistent indexing of NBD patterns from arbitrarily oriented nanocrystals and retrieves their orientations. The method opens the door to a thorough characterization of nanocrystalline structures in wire, film, and bulk materials and is an essential step to a more quantitative understanding of the structure−property relationships of nanocrystalline materials.

As an example material, we use nanocrystalline copper bulk, which is, at present, in the focus of discussion due to its special properties.[3,4] For the first time, orientation information of larger areas of adjacent nanograins is collected, providing a grain boundary analysis on the nanoscale with some statistical evaluation.

Orientation Determination Algorithm. The misorientation between two adjacent grains determines the energetic state and the mobility of the grain boundary between them.[34] A grain boundary is defined by a misorientation angle and a misorientation axis.[35] To determine the misorientation relationship, first the orientation matrix of each grain is determined from

its diffraction pattern. The orientation matrix describes a grain's orientation ($\mathbf{x_C}$, $\mathbf{y_C}$, $\mathbf{z_C}$) with respect to the reference coordinate system ($\mathbf{x_R}$, $\mathbf{y_R}$, $\mathbf{z_R}$), for example, the sample frame (Figure1). The misorientation matrix is calculated from the orientation matrices of two adjacent grains.[35,36]

Due to nearly parallel illumination, a NBD pattern consists of small diffraction disks with a uniform intensity.[20] Kossel line features that are commonly used for orientation determination in TEM[29] are not contained. Using NBD, a grain's orientation is determined only from the positions of the diffraction disks. Due to the low thickness of the nanocrystals, the NBD pattern dimensions and intensities can be interpreted similarly as for a spot pattern in selected area diffraction (SAD).[21,23] Thus, methods to index SAD patterns[37] are adapted here to analyze the NBD patterns. The orientation matrix is calculated using a procedure that is commonly used for Kikuchi diffraction.[36,38,39] A computer algorithm was developed that facilitates unique indexing of NBD patterns from random orientated grains as well as calculation of their orientation matrix. As a first step, the length of the diffraction vectors and their angular relations are quantified from five selected diffraction disks in the NBD pattern. The indexing is based on the comparison of the theoretical vector lengths and angles with the quantified values.[37] The indexing is verified by the method of Ryder and Pitsch.[40] Afterward, the normal direction **r** is calculated that is antiparallel to the electron beam. Owing to the relrod geometry of the reciprocal lattice points (induced by the finite thickness of the TEM foil), a NBD pattern of a random orientated grain contains several diffraction disks of different zero-order Laue zones.[20] The **r** is determined by the equation of Ryder and Pitsch[40] that averages the Laue conditions of three diffraction vectors belonging to different zones:

$$\mathbf{r} = |\mathbf{g}_1|^2(\mathbf{g}_2 \times \mathbf{g}_3) + |\mathbf{g}_2|^2(\mathbf{g}_3 \times \mathbf{g}_1) + |\mathbf{g}_3|^2(\mathbf{g}_1 \times \mathbf{g}_2) \quad (1)$$

To get a good estimate of **r** and finally of the orientation matrix **M**, the five diffraction vectors are split in two vector triples, where the first vector is identical in both triples. Thus, two different normal directions **r** are calculated.

The orientation matrix **M** is obtained by a two-step process based on the procedure described in refs 38 and 39 (Figure 1). First, a pattern frame ($\mathbf{x_P}$, $\mathbf{y_P}$, $\mathbf{z_P}$) is defined with the *z*-axis parallel to **r** and the *y*-axis $\mathbf{y_P}$ parallel to $\mathbf{r} \times \mathbf{g}$, where **g** is any diffraction vector ($\mathbf{g_2}$ in Figure 1). The rotation matrix $\mathbf{R_{CP}}$ from the crystal to the pattern frame is given by

$$\mathbf{R_{CP}} = \begin{pmatrix} (\mathbf{r} \times \mathbf{g}) \times \mathbf{r} \\ \mathbf{r} \times \mathbf{g} \\ \mathbf{r} \end{pmatrix} \quad (2)$$

The pattern frame ($\mathbf{x_P}$, $\mathbf{y_P}$, **r**) and the reference frame ($\mathbf{x_R}$, $\mathbf{y_R}$, **r**) differ only by a right-handed rotation of

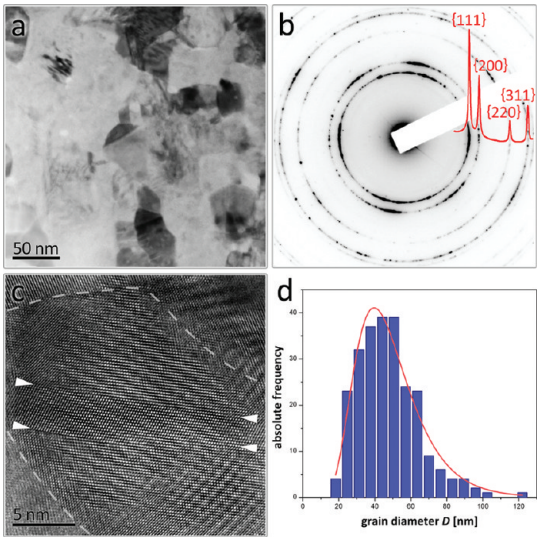

Figure 2. TEM images and grain size distribution of the nc-Cu sample: (a) bright-field image showing the typical nc-Cu microstructure. (b) Selected area diffraction pattern indicating a slight crystallograpihc texture; inset indexed radial averaged intensity distribution. (c) HRTEM image of a nanograin containing a twin, with dashed lines indicating nanograin boundaries and arrows indicating twin boundaries. (d) Measured grain size distribution and fit with a log-normal distribution; the mean grain size is ~46 nm.

φ around **r**, where φ is the angle between $\mathbf{x_P}$ and $\mathbf{x_R}$ (Figure1). The corresponding rotation matrix is

$$\mathbf{R_{PR}} = \begin{pmatrix} \cos\varphi & \sin\varphi & 0 \\ -\sin\varphi & \cos\varphi & 0 \\ 0 & 0 & 1 \end{pmatrix} \quad (3)$$

Finally, the combined rotations of eqs 2 and 3 are equivalent to the rotation from crystal to reference:

$$\mathbf{R_{CR}} = \mathbf{R_{PR}} \times \mathbf{R_{CP}} \quad (4)$$

In order to be consistent with the definition of the orientation matrix given by Bunge,[35] the orientation matrix **M** that represents the rotation from the reference to crystal frame is the transpose of $\mathbf{R_{CR}}$. For increasing the accuracy, the orientation matrix **M** is taken as the average of four calculated solutions resulting from two calculated normal directions **r** and by selecting two different diffraction vectors **g**.

The misorientation matrix of two neighboring grains can be determined from their orientation matrices $\mathbf{M_1}$ and $\mathbf{M_2}$

$$\mathbf{M}_{12} = \mathbf{M}_2^{-1} \times \mathbf{M}_1 \quad (5)$$

The obtained misorientation matrix allows the calculation of the misorientation axis angle pair.[35]

Angular Resolution of the NBD Analysis. The accuracy of the angular resolution of the NBD analysis for determining the orientation of a grain in space is not quite as good as EBSD. Due to the low film thickness, the NBD pattern can be regarded as a kinematical disk pattern. This type of pattern is not as sensitive against tilting as

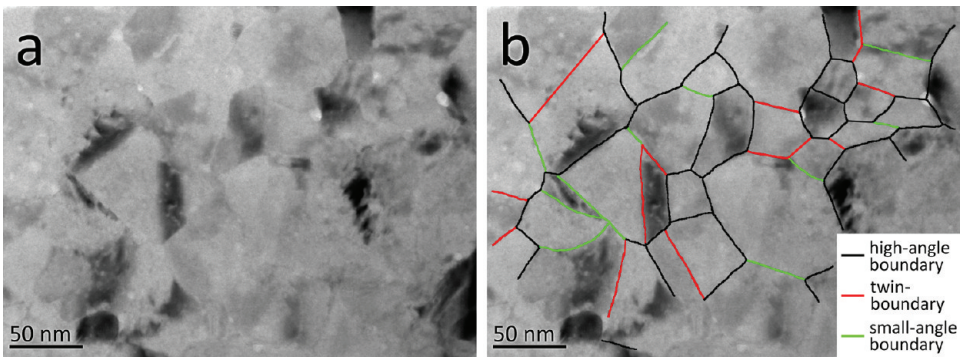

Figure 3. Grain boundary network in the nc-Cu sample: (a) bright-field image of a sample part that was analyzed using NBD; (b) microstructure superposed with the analyzed grain boundary network; twin and small-angle boundaries are displayed in red and green, respectively.

dynamical (Kikuchi) patterns used in EBSD. However, using three diffraction spots for orientation determination, the precision of the algorithm is better than 3° if it is applied to a SAD spot pattern.[40] To achieve a higher precision, the algorithm calculates the orientation from five diffraction spots. A further source of uncertainty is the broadening of the reciprocal lattice points due to the nanoscale size of the observed grains. The broader reciprocal lattice points intersect the Ewald sphere over a larger angular range, yielding a lower possible accuracy in orientation determination. The highest possible accuracy is achieved if the selected diffraction disks in the NBD pattern display high intensity and are located far from the center. The high intensity implies that the diffraction disk is close to the ideal Bragg condition. A larger distance of a disk from the center increases the accuracy of orientation determination because its appearance is more sensitive to grain orientation. Following these two rules and using the angle between the two calculated normal directions **r** of the NBD pattern as a measure of accuracy, the angular uncertainty is usually below 2°. As a "worst case scenario", the angular resolution could be reduced to about 4° in very few instances, depending on the orientation of the grain to the electron beam and the experience of the operator. Identifying *relative* orientation deviations between neighboring grains is possible to <2° by selecting the unique spots of the respective diffraction pattern of each grain. Accordingly, the achieved accuracy is in the same order as that from EBSD analysis.

RESULTS

In Figure 2, an overview of the grain structure of nc-Cu (Figure 2a), the corresponding diffraction pattern (Figure 2b), a high-resolution TEM image (HRTEM) of a twin in a nanograin (Figure 2c), and the grain size distribution (Figure 2d) are shown. The measured grain size distribution of 248 grains (Figure 2c) is well represented by a log-normal distribution with a mean grain size of ~46 nm. The nc-Cu sample contains numerous grains and twin structures whose grain

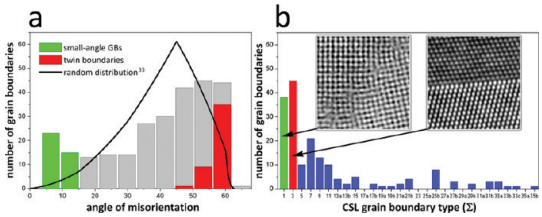

Figure 4. Statistical evaluation of the grain boundaries in nc-Cu: (a) misorientation angle distribution of 268 analyzed grain boundaries, in comparison with a random distribution;[34] (b) grain boundary character distribution of the identified CSL boundaries; twin and small-angle boundaries are displayed in red and green, respectively.

boundary character cannot be determined by methods that are available at present. The intensity maxima on the diffraction rings (Figure 2b) indicate a slightly textured structure.

The method described above was used to determine the distributions of misorientation angles and misorientation axes between adjacent grains. A more detailed image of the grain structure is shown in Figure 3a. The contrast between grains in the nc-Cu is relatively weak. With the NBD method, grain boundary characters were determined and added to the micrograph (Figure 3b), providing for the first time a direct link between texture and microstructure in a nanocrystalline material with a grain size well below 50 nm. Note that numerous boundaries are marked as twin boundaries that cannot be identified as such from the micrograph in Figure 3a. Compared to a visual inspection of micrographs, the quantitative analysis using NBD is unambiguous and consistent and thus gives more reliable insight into the microstructural features.

The grain boundary symmetry is described here using the concept of coincidence site lattice (CSL) using the nearness condition after Brandon.[41] It is pertinent to note that the CSL concept does not provide a complete characterization of the grain boundary, due to the lack of information about the boundary plane orientation. Even though it has only a practical implication for special boundary types with a particular orientation, it is generally accepted for

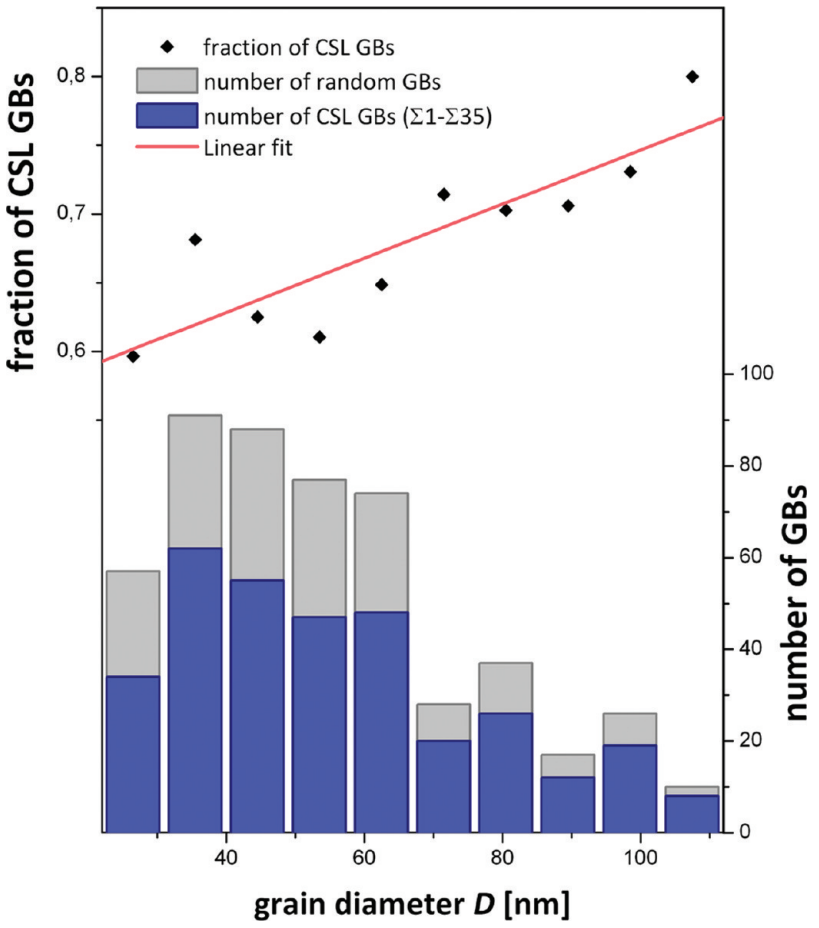

Figure 5. Fraction of CSL boundaries (Σ1−Σ35) plotted against grain size including the corresponding distribution of the number of CSL and random grain boundaries (blue and gray) analyzed with NBD; the slope of the linear fit shows that the grain boundary character depends on the grain size.

geometrical classification of the grain boundaries. The variable Σ corresponds to the reciprocal density of coincidence points between the lattices of adjacent grains. The grain boundaries are classified in four categories based on the misorientation between the neighboring grains. Small-angle boundaries of less than 15° misorientation are considered as Σ1 boundaries. Twin boundaries are classified as Σ3. Grain boundaries with Σ5 to Σ35 are considered as low Σ (or special) boundaries, and random high-angle boundaries are those with Σ above 35.

The misorientation angle distribution and the grain boundary character distribution of a nanocrystalline material are shown in Figure 4, allowing a statistical evaluation. The misorientation angle distribution (Figure 4a) obtained from 268 grain boundaries shows a bimodal character and is thus clearly different from a random distribution of a texture free material (solid line in Figure 4a).[42] It is obvious that the peak at low misorientation angles results from the high fraction of small-angle grain boundaries (Σ1). A comparison with the grain boundary character distribution (Figure 4b) shows that the maximum at *ca.* 60° is caused by the high fraction of twin boundaries (Σ3), a consequence of the low stacking-fault energy in copper. Hence, the texture observed in the SAD pattern in Figure 2b correlates with the high fraction of twin and small-angle boundaries. These types of boundaries are regarded as stable and unfavorable for grain growth;[10] they contribute to the thermal stability of nc-Cu together with possible thermodynamic reasons as, for example, specified in ref 11.

In contrast, Cu with a mean grain size on the order of 210 nm produced by equal channel angular pressing[43] starting from high-purity Cu exhibits a nearly random misorientation angle distribution. In addition to possible differences due to the grain size, we attribute the difference in the misorientation angle distribution between the two cases to the different purities of the corresponding raw materials. Higher purity yields a higher stacking-fault energy[44] that results in a lower twinning probability and thus in a more random misorientation angle distribution.

For quantifying the spatial distribution of twin and small-angle boundaries in the microstructure, the data of the grain size and the grain boundary analyses are correlated. To obtain a higher statistical confidence, not only twin and small-angle boundaries but all CSL

boundary types ($\Sigma1-\Sigma35$) were evaluated. In Figure 5, the fraction of these boundaries is plotted against the size of the adjacent grains. The columns display the number of CSL grain boundaries (blue) and random grain boundaries (gray) surrounding the grains of the relevant classes of grain size. For geometric reasons (since a boundary connects two adjacent grains), each grain boundary is counted twice. The distribution of all grain boundaries (blue and gray) over the grain size (Figure 5) follows a log-normal function with the same characteristics as the grain size distribution (Figure 2c), confirming that the grains analyzed with NBD are representative for the microstructure. The data points in Figure 5 describe the fraction of CSL boundaries in the corresponding grain size class. The slope of the linear fit (Figure 5) indicates that the fraction of twin and small-angle boundaries decreases with decreasing grain size. This is certainly an unexpected and novel result. In other words, the smaller grains possess more random high-angle boundaries. Thus, the grain boundary character depends sensitively on the grain size. Extrapolation of measured orientation relationships from structures on the mesoscale to nanomaterials and even extrapolation within the nanoscale appears to be problematic, as nanostructures require detailed analysis for each mean grain size and grain size distribution.

The resolution of the NBD method is further enhanced to below 1 nm if a TEM equipped with a field emission gun[23,30] is used. The accuracy of measured misorientation angles is on the order of 2°; thus, the angular resolution is slightly lower than that of EBSD, but the spatial resolution is higher by at least 1 order of magnitude. With the exception of the orientation of the grain boundary *plane* that requires additional NBD patterns in a second sample orientation,[38] the presented NBD method offers the opportunity to a complete characterization of a nanoscale grain structure.

In summary, we developed a novel method that allows characterization of nanostructures concerning grain and twin boundaries that are generally accepted to be the cause of the special properties of nanocrystalline materials. The method is based on quantitative nanobeam diffraction in transmission electron microscopy and is capable of determining the misorientation of adjacent nanograins, subgrains, and nanotwins. Spatial resolution of <5 nm has been achieved, as demonstrated in nanocrystalline Cu. The results indicate that there is a dependence of the grain boundary character in nanocrystalline materials on the grain size. Thus, extrapolation of measured orientation relationships from structures on the mesoscale to nanoscale appears to be disputable. The understanding of the structure−property relationship of nanostructured materials should be based on precise orientation analysis of nanocrystals.

METHODS

Sample Preparation. The nc-Cu was prepared by a powder metallurgy method that combines the high-energy ball milling and the spark plasma sintering (SPS). In order to avoid introducing contaminations, the preparation procedures were all performed in an entirely closed system filled with highly purified argon gas.[45] Cu powder with a purity of 99.5% and a mean diameter of 10 μm was used as raw material. First, high-energy ball milling was performed on the Cu powder in a Fritsch Pulverisette 7 planetary ball mill at a speed of 400 rpm for 30 h. Subsequently, the milled Cu powder was loaded in a die made of cemented carbides and transferred inside the glovebox to the sintering chamber of the SPS equipment (SPS-5.40MK-IV). The sintering parameters were as follows: final sintering temperature 623 K, heating rate 50 K/min, and no isothermal holding time. The sintering pressure was kept constant at 500 MPa for the whole SPS process. The relative density of the sintered nc-Cu bulk sample was measured as 99.5% by the Archimedes method using absolute alcohol as the liquid medium. X-ray diffraction (XRD) analysis showed that the as-prepared Cu bulk sample is single phase and consists of fcc Cu.

From the nc-Cu bulk sample, TEM foils were prepared using mechanical grinding followed by dimple grinding and low-angle Ar-ion milling.

Electron Microscopy. The TEM observation was carried out using a JEM 3010 TEM/STEM (HR pole piece, JEOL) equipped with a multiscan 1k × 1k charge-coupled device (CCD) camera (Gatan). The NBD mode was operated with a beam diameter of 5 nm, the alpha-selector 1, and the smallest available condenser aperture (10 μm). The corresponding convergence angle 2α was determined experimentally[20] to be less than 1 mrad, providing the required nearly parallel beam. The diffraction patterns of each single nanograin were recorded using a camera length of 20 cm to include a larger area of the diffraction pattern. The camera length was calibrated carefully using a single crystalline sample of pure Si. The TEM bright-field image with arbitrary orientation of the sample (Figure 2a) shows some regions where grain shapes and grain boundaries can be clearly distinguished, along with other regions of poor diffraction contrast between adjacent grains, that is, hardly visible grain boundaries. To clearly identify all grain boundaries, the sample was tilted in the range of ±5° to produce a change of diffraction conditions and thus enhance the contrast locally. For each grain, at least two NBD patterns were recorded at different positions to avoid artifacts, for example, resulting from grain overlap or sample drift. Furthermore, the electron beam was shifted from each grain to all adjacent grains while observing the NBD patterns to prove neighboring relation by the abrupt change of the NBD pattern. Finally, the orientation of each grain was determined from its NBD pattern using the method introduced above, implemented in a software code that is written within the software Digital micrograph (Gatan). Overall, 118 NBD patterns originating from three different sample positions were analyzed, yielding 268 orientation relationships. As a measure for the grain size and grain size distribution, the equivalent circular diameter of grain projected area was used.[46]

Acknowledgment. Stimulating discussions with Prof. A. Chuvilin (CIC, San Sebastian, Spain), Dr. U. Bläss, and Prof. H.-G. Leopold (FSU Jena) and assistance from Dr. W. Tirschler (TU Dresden) for the misorientation calculations are gratefully acknowledged. Financial support is acknowledged from DFG (Grant Re1261/9) and by one of the authors (X.Y.S.) from the National Natural Science Foundation of China (Grant No. 50871001).

REFERENCES AND NOTES

1. Dao, M.; Lu, L.; Asaro, R. J.; De Hosson, J. T. M.; Ma, E. Toward a Quantitative Understanding of Mechanical Behavior of Nanocrystalline Metals. *Acta Mater.* **2007,** *55*, 4041–4065.
2. Farkas, D.; Hyde, B. Improving the Ductility of Nanocrystalline BCC Metals. *Nano Lett.* **2005,** *5*, 2403–2407.
3. Lu, K.; Lu, L.; Suresh, S. Strengthening Materials by Engineering Coherent Internal Boundaries at the Nanoscale. *Science* **2009,** *324*, 349–352.
4. Lu, L.; Shen, Y. F.; Chen, X. H.; Qian, L. H.; Lu, K. Ultrahigh Strength and High Electrical Conductivity in Copper. *Science* **2004,** *304*, 422–426.
5. Zhang, X.; Anderoglu, O.; Hoagland, R. G.; Misra, A. Nanoscale Growth Twins in Sputtered Metal Films. *J. Min. Metall. Mater. Soc.* **2008,** *60*, 75–78.
6. Gleiter, H. Nanostructured Materials: Basic Concepts and Microstructure. *Acta Mater.* **2000,** *48*, 1–29.
7. Valiev, R. Nanostructuring of Metals by Severe Plastic Deformation for Advanced Properties. *Nat. Mater.* **2004,** *3*, 511–516.
8. Van Swygenhoven, H.; Derlet, P. M.; Froseth, A. G. Stacking Fault Energies and Slip in Nanocrystalline Metals. *Nat. Mater.* **2004,** *3*, 399–403.
9. Yamakov, V.; Wolf, D.; Phillpot, S. R.; Mukherjee, A. K.; Gleiter, H. Deformation-Mechanism Map for Nanocrystalline Metals by Molecular-Dynamics Simulation. *Nat. Mater.* **2004,** *3*, 43–47.
10. Gottstein, G.; Shvindlerman, L. S. On the Orientation Dependence of Grain-Boundary Migration. *Scr. Metall. Mater.* **1992,** *27*, 1515–1520.
11. Song, X. Y.; Zhang, J. X.; Li, L. M.; Yang, K. Y.; Liu, G. Q. Correlation of Thermodynamics and Grain Growth Kinetics in Nanocrystalline Metals. *Acta Mater.* **2006,** *54*, 5541–5550.
12. Li, Q. G.; Penner, R. M. Photoconductive Cadmium Sulfide Hemicylindrical Shell Nanowire Ensembles. *Nano Lett.* **2005,** *5*, 1720–1725.
13. Wang, J. G.; Tian, M. L.; Kumar, N.; Mallouk, T. E. Controllable Template Synthesis of Superconducting Zn Nanowires with Different Microstructures by Electrochemical Deposition. *Nano Lett.* **2005,** *5*, 1247–1253.
14. Gruen, D. M. Nanocrystalline Diamond Films. *Annu. Rev. Mater. Sci.* **1999,** *29*, 211–259.
15. Bhattacharyya, S.; Auciello, O.; Birrell, J.; Carlisle, J. A.; Curtiss, L. A.; Goyette, A. N.; Gruen, D. M.; Krauss, A. R.; Schlueter, J.; Sumant, A.; Zapol, P. Synthesis and Characterization of Highly-Conducting Nitrogen-Doped Ultrananocrystalline Diamond Films. *Appl. Phys. Lett.* **2001,** *79*, 1441–1443.
16. Van Swygenhoven, H. Polycrystalline Materials: Grain Boundaries and Dislocations. *Science* **2002,** *296*, 66–67.
17. Humphreys, F. J. Characterisation of Fine-Scale Microstructures by Electron Backscatter Diffraction (EBSD). *Scr. Mater.* **2004,** *51*, 771–776.
18. Zaefferer, S. On the Formation Mechanisms, Spatial Resolution and Intensity of Backscatter Kikuchi Patterns. *Ultramicroscopy* **2007,** *107*, 254–266.
19. Park, N. J.; Field, D. P.; Nowell, M. M.; Besser, R. Effect of Film Thickness on the Evolution of Annealing Texture in Sputtered Copper Films. *J. Electron. Mater.* **2005,** *34*, 1500–1508.
20. Williams, D. B.; Carter, C. B. *Transmission Electron Microscopy: A Textbook for Materials Science*; Plenum Press: New York, 1996; p xxvii, 729 pp.
21. Cowley, J. M. Electron Nanodiffraction. *Microsc. Res. Tech.* **1999,** *46*, 75–97.
22. Cowley, J. M.; Spence, J. C. H. Convergent Beam Electron Microdiffraction from Small Crystals. *Ultramicroscopy* **1981,** *6*, 359–366.
23. Cowley, J. M. Applications of Electron Nanodiffraction. *Micron* **2004,** *35*, 345–360.
24. Li, C. F.; Williams, D. B. Application of Automated Crystallography for Transmission Electron Microscopy in the Study of Grain-Boundary Segregation. *Micron* **2003,** *34*, 199–209.
25. Dingley, D. J.; Nowell, M. M. The Use of Electron Backscatter Diffraction for the Investigation of Nano Crystalline Materials and the Move towards Orientation Imaging in the TEM. *Microchim. Acta* **2004,** *147*, 157–165.
26. Dingley, D. J. Orientation Imaging Microscopy for the Transmission Electron Microscope. *Microchim. Acta* **2006,** *155*, 19–29.
27. Wu, G. L.; Zaefferer, S. Advances in Tem Orientation Microscopy by Combination of Dark-Field Conical Scanning and Improved Image Matching. *Ultramicroscopy* **2009,** *109*, 1317–1325.
28. Zschech, E.; Huebner, R.; Chumakov, D.; Aubel, O.; Friedrich, D.; Guttmann, P.; Heim, S.; Schneider, G. Stress-Induced Phenomena in Nanosized Copper Interconnect Structures Studied by X-ray and Electron Microscopy. *J. Appl. Phys.* **2009,** *106*, 5.
29. Fundenberger, J. J.; Morawiec, A.; Bouzy, E.; Lecomte, J. S. Polycrystal Orientation Maps from TEM. *Ultramicroscopy* **2003,** *96*, 127–137.
30. Alloyeau, D.; Ricolleau, C.; Oikawa, T.; Langlois, C.; Le Bouar, Y.; Loiseau, A. STEM Nanodiffraction Technique for Structural Analysis of CoPt Nanoparticles. *Ultramicroscopy* **2008,** *108*, 656–662.
31. Rauch, E. F.; Portillo, J.; Nicolopoulos, S.; Bultreys, D.; Rouvimov, S.; Moeck, P. Automated Nanocrystal Orientation and Phase Mapping in the Transmission Electron Microscope on the Basis of Precession Electron Diffraction. *Z. Kristallogr.* **2010,** *225*, 103–109.
32. Ganesh, K. J.; Kawasaki, M.; Zhou, J. P.; Ferreira, P. J. D-Stem: A Parallel Electron Diffraction Technique Applied to Nanomaterials. *Microsc. Microanal.* **2010,** *16*, 614–621.
33. Paul, H.; Morawiec, A.; Bouzy, E.; Fundenberger, J. J.; Piatkowski, A. Orientation Imaging in Scanning Electron and Transmission Electron Microscopy for Characterization of the Shear Banding Phenomenon. *Microchim. Acta* **2006,** *155*, 243–250.
34. Wolf, D.; Yamakov, V.; Phillpot, S. R.; Mukherjee, A.; Gleiter, H. Deformation of Nanocrystalline Materials by Molecular-Dynamics Simulation: Relationship to Experiments? *Acta Mater.* **2005,** *53*, 1–40.
35. Randle, V.; Engler, O. *Introduction to Texture Analysis: Macrotexture, Microtexture and Orientation Mapping*; Gordon and Breach Science Publishers: Amsterdam, The Netherlands, 2000; p 388.
36. Lange, F. F. Mathematical Characterization of a General Bicrystal. *Acta Metall. Mater.* **1967,** *15*, 311–318.
37. Zaefferer, S. New Developments of Computer-Aided Crystallographic Analysis in Transmission Electron Microscopy. *J. Appl. Crystallogr.* **2000,** *33*, 10–25.
38. Young, C. T.; Steele, J. H.; Lytton, J. L. Characterization of Bicrystals Using Kikuchi Patterns. *Metall. Trans.* **1973,** *4*, 2081–2089.
39. Heilmann, P.; Clark, W. A. T.; Rigney, D. A. Computerized Method To Determine Crystal Orientations from Kikuchi Patterns. *Ultramicroscopy* **1982,** *9*, 365–371.
40. Ryder, P. L.; Pitsch, W. On Accuracy of Orientation Determination by Selected Area Electron Diffraction. *Philos. Mag. A* **1968,** *18*, 807.
41. Brandon, D. G. Structure of High-Angle Grain Boundaries. *Acta Metall. Mater.* **1966,** *14*, 1479–1484.
42. Mackenzie, J. K. 2nd Paper on Statistics Associated with the Random Disorientation of Cubes. *Biometrika* **1958,** *45*, 229–240.
43. Mishin, O. V.; Gertsman, V. Y.; Valiev, R. Z.; Gottstein, G. Grain Boundary Distribution and Texture in Ultrafine-Grained Copper Produced by Severe Plastic Deformation. *Scr. Mater.* **1996,** *35*, 873–878.
44. Kapoor, K.; Lahiri, D.; Batra, I. S.; Rao, S. V. R.; Sanyal, T. X-ray Diffraction Line Profile Analysis for Defect Study in Cu-1 wt. % Cr-0.1 wt.% Zr Alloy. *Mater. Charact.* **2005,** *54*, 131–140.
45. Song, X. Y.; Zhang, J. X.; Yue, M.; Li, E. D.; Zeng, H.; Lu, N. D.; Zhou, M. L.; Zuo, T. Y. Technique for Preparing Ultrafine Nanocrystalline Bulk Material of Pure Rare-Earth Metals. *Adv. Mater.* **2006,** *18*, 1210–1215.
46. Seyring, M.; Song, X.; Chuvilin, A.; Kaiser, U.; Rettenmayr, M. Characterization of Grain Structure in Nanocrystalline Gadolinium by HRTEM. *J. Mater. Res.* **2009,** *24*, 342–346.